Monolithically Integrated Light Feedback Control Circuit for Blue/UV LED Smart Package

Koladouz Esfahani, Zahra; Tohidian, Massoud; Van Zeijl, Henk; Kolahdouz, Mohammadreza; Zhang, Guoqi

DOI
10.1109/JPHOT.2017.2677580

Publication date
2017

Document Version
Final published version

Published in
IEEE Photonics Journal

IEEE Photonics Journal
An IEEE Photonics Society Publication

Open Access

Monolithically Integrated Light Feedback Control Circuit for Blue/UV LED Smart Package

Volume 9, Number 2, April 2017

Zahra Kolahdouz Esfahani, *Student Member, IEEE*
Massoud Tohidian, *Member, IEEE*
Henk van Zeijl, *Member, IEEE*
Mohammadreza Kolahdouz, *Member, IEEE*
Guoqi Zhang, *Fellow, IEEE*

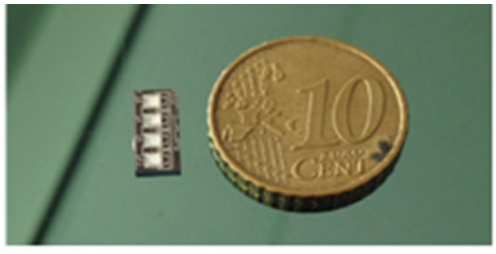

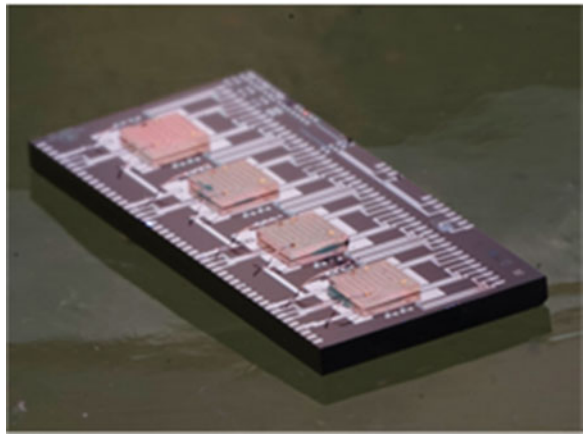

DOI: 10.1109/JPHOT.2017.2677580
1943-0655

IEEE photonics SOCIETY

IEEE

Monolithically Integrated Light Feedback Control Circuit for Blue/UV LED Smart Package

Zahra Kolahdouz Esfahani,[1] ***Student Member, IEEE*****,**
Massoud Tohidian,[1] ***Member, IEEE*****, Henk van Zeijl,**[1] ***Member, IEEE*****,**
Mohammadreza Kolahdouz,[2] ***Member, IEEE*****,**
and Guoqi Zhang,[1] ***Fellow, IEEE***

[1]Electrical Engineering Department, Delft University of Technology, Delft 2628CT, The Netherlands
[2]School of Electrical and Computer Engineering, University of Tehran, Tehran 14174-66191, Iran

DOI:10.1109/JPHOT.2017.2677580

Manuscript received January 18, 2017; revised February 24, 2017; accepted February 28, 2017. Date of publication March 3, 2017; date of current version March 23, 2017. Corresponding author: Zahra Kolahdouz Esfahani (z.kolahdouzesfahani@tudelft.nl).

Abstract: Given the performance decay of high-power light-emitting diode (LED) chips over time and package condition changes, having a reliable output light for sensitive applications is a point of concern. In this study, a light feedback control circuit, including blue-selective photodiodes, for blue/ultraviolet (UV) LED, has been designed and implemented using a low-cost seven-mask BiCMOS process. The feedback circuit was monolithically integrated in a package with four high-power blue LED chips. For sensing the intensity of exact colored blue/UV light in the package, selective photodiodes at 480-nm wavelength were implemented. An opamp-based feedback circuit combined with a high-power transistor controls the output light based on real-time sensor data. The whole system is a low-cost integrated package that guarantees a stable and reliable output light under different working conditions. Output light can be also controlled linearly by a reference input voltage.

Index Terms: Blue/ultraviolet (UV) light-emitting diode (LED), BiCMOS process, photodetector, high current CMOS transistor, feedback control, wafer level LED package.

1. Introduction

Introducing high power light-emitting diodes (LEDs) was a key step for development of new application areas in lighting such as sustainable lighting, general interior and exterior illumination, backlighting for displays, smart lighting (e.g., data transportation), indicators and signs, non-visual applications (communication), and transportation equipment lighting [1]–[4].

The most common approach for high power white LED source is the dichromatic method, which is also entitled as phosphor-based white method. It is a combination of a short wavelength LED, such as blue or UV, and phosphoric wavelength shifter. In the phosphor coating, a portion of photons are converted to yellow and the rest travel without any change. The light output is seen as a white light by human eyes [1]–[3]. This method shows good color rendering, long lifetime and acceptable reliability over the time. However, aging and high junction temperature affect emitting wavelength and intensity [4]–[6]. This degradation may refer both to phosphor and LED chip performance over

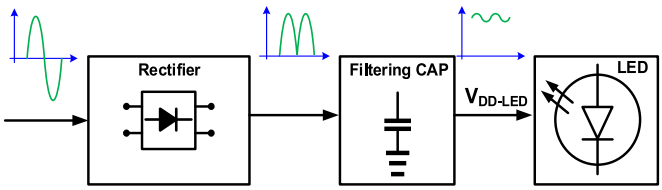

Fig. 1. Block diagram of AC to DC converter used in LED packages. A fast light feedback system can suppress the ripples on V_{DD_LED}.

the time. While phosphor working mechanism is related to the manufacturing process [1], we can compensate LED aging and adjust its light intensity by controlling its driving current in a closed-loop system [7].

Another concern is large heat dissipation in such a high power package. Silicon wafer-level-package (WLP) can be a good solution for thermal management and a cost effective integration [6], [8], [9]. Using silicon-based infrastructures, IC technologies, and MEMS toolset and processes allows us to integrate different functional sub-blocks on the same die.

Monolithic integration of photonics and electronics in Si and other group IV elements was previously demonstrated [10]–[12]. Different groups reported integration of sensors and controlling blocks in Si-based LED WLP [6], [13]–[15]. However, developing a complete real-time light output controlling block in a low-cost process is still a point of interest.

To address the above issues, a light feedback control system including sensors, control circuit, and power transistor for driving LED is monotonically integrated in a low-cost process. It controls the light output of the package with a real-time feedback signal from light sensor that receives emitted blue light of LED chips. The fabrication is done through a simple and low-cost 7-mask BiCMOS process (BiCMOS7). This integrated package incorporates a blue selective photodiode (as the light sensor) that was previously published by the authors [7]. Implementation of sensors (and potentially rectifier) requires a BJT process. The best process choice for the analog/digital control circuit is CMOS. Therefore, we used a BiCMOS process for monolithic integration of this system. The package guarantees a stable light output that is linearly controllable with a reference input voltage.

This paper is organized as follow: in Section 2, system level design of feedback control circuit is discussed which explains: feedback circuit, design of operational amplifier (opamp), power transistor, target LED, and the blue selective photo diodes. Section 3 summarizes system implementation. In Section 4, test procedure and measurement results are deliberated. Finally, the conclusion is in Section 4.

2. System-Level Design of Feedback Control Circuit

A control box for a smart LED package should fulfill several considerations:

1) Stability of the light intensity and color temperature against different working conditions: If, due to any reason, such as increased package temperature, there is decay in intensity and a shift in color, the feedback circuit must keep the blue index of light output at desired value.
2) Compensation for aging effects of LED chips: According to the lifetime prediction of LED chips from some of the manufacturing companies [16], [17], the performance decays critically over the time. Although phosphor and material aging cannot be controlled electrically, package aging can be partially recompensed by controlling the driving current.
3) Dimming the light output intensity with a reference input: In some applications, it is necessary to have a reliable level of light output with dimming capability controlled by an extra reference value.
4) Filtering ripples of power supply: Usually, power voltage of LED is provided by a rectifier from an AC source (an example is shown in Fig. 1). To have a stabilized light output of the LED package, the rectified signal is then filtered with a capacitor to reduce its ripples. However,

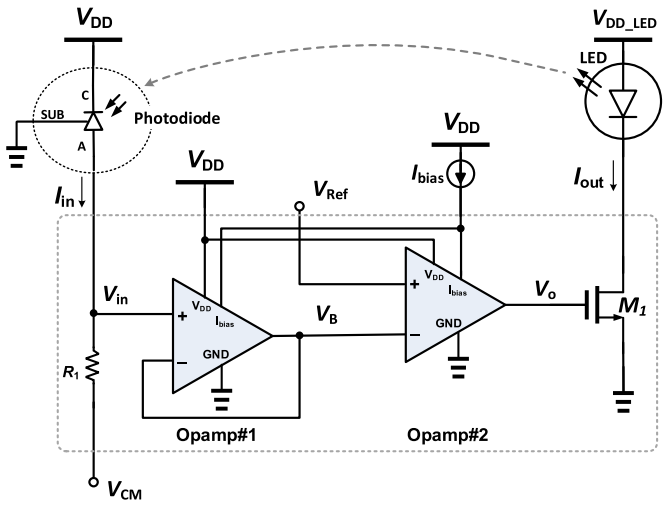

Fig. 2. Schematic of light feedback control circuit.

a good and clean DC signal requires a large capacitor which increases the cost. As studies have reported [18]–[20], LED voltage and current ripples can decrease efficacy (lm/W) up to 4%. Moreover, if dissipated power of the LED is not regulated, a high ripple may increase the LED junction temperature. This ripple can be substantially removed with a fast enough feedback circuit and avoids any efficacy degradation. Hence, the filtering capacitor can be also smaller/cheaper. Moreover, it enables further integration of this capacitor that can result in additional cost reduction.

Using a linear feedback circuit that monitors selectively blue light output of the LED tackles all these concerns. This control circuit has been integrated together with a driving power transistor into the silicon package of LED to reduce cost and increase reliability.

2.1 Feedback Circuit

The control circuit basically consists of 2 operational amplifiers (opamp) and a power transistor. It is schematically shown in Fig. 2. The input is a current signal from the blue selective photodiode, which instantly senses the light output of LED chip and turns it into current (I_{in}). This current makes a voltage drop over a 40 kΩ resistor (R_1) that is biased over a common-mode voltage (V_{CM}). Input voltage (V_{in}) is then buffered through the first opamp (V_B). This buffer stage avoids any unwanted capacitive loading in the sensing circuit. It also provides reverse isolation from output of the second opamp with a high gain to the sensitive (high impedance) node of the sensor (V_{in}) and improves loop stability. In the second stage, V_B is compared with a reference voltage (V_{Ref}) and then amplified with a very high gain (>200x). The output voltage (V_O) is then fed to a power transistor (M_1). This transistor drains a current through the LED from V_{DD_LED}.

Polarity of the whole feedback is set in a way to make a negative feedback loop. The photodiode senses intensity of the blue light emitted from the LED. The higher LED light intensity, the higher photocurrent (I_{in}). Therefore, it increases V_{in} and consequently V_B. This is then compared with V_{Ref} and amplified with a high negative gain. Hence, V_O is decreased. This reduces the drain current of the power transistor and in turn reduces and regulates the LED light intensity.

As the loop has a very high gain, it can be assumed that V_B (and V_{in}) is forced by the feedback to be equal to V_{Ref}. Therefore, we can have the following equation:

$$V_{in} = R_1 \times I_{in} + V_{CM} = V_{Ref} \Rightarrow I_{in} = \frac{V_{Ref} - V_{CM}}{R_1}. \quad (1)$$

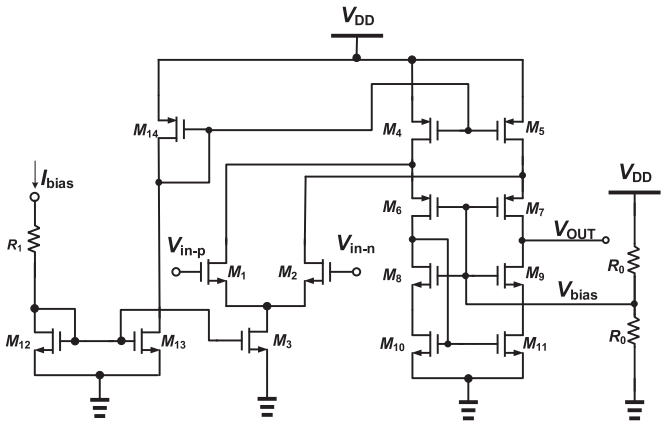

Fig. 3. Schematic of designed folded cascode opamp.

Since I_{in} is a linear function of its input light intensity, light output of the LED is a linear function of the reference input voltage V_{Ref}.

2.2 Opamp

For the feedback control circuit, a high gain opamp structure is required to minimize feedback error. The first option can be a single stage opamp which has a good frequency stability. However, it cannot provide a high gain (<30 dB in our used process). Aiming a higher gain, there are two common options: cascode and two-stage structures [21], [22]. Although the two-stage structure provides a very high gain and excellent input common-mode (CM) range, it suffers from poor stability that makes frequency compensation techniques unavoidable. Thus, the cascode structure was chosen, which does not require any frequency compensation and has a single-pole like transfer function. This is very important to make the whole feedback system stable.

Implementation wise, telescopic cascode structure [21], [22] eats up all the voltage headroom for input CM range and output swing. Therefore, for the final implementation, folded-cascode structure (see Fig. 3) was chosen. It can have a high input CM range with good enough output swing for our application. Additionally, it provides a high power supply rejection ratio (PSRR) [22] that makes supply variations less of a concern. The folded-cascode structure has an inferior noise performance compared to both telescopic cascode and two-stage structures. This is mainly due to the additional current source used for folding ($M_{4,5}$). However, noise level of this opamp structure is still quite low for general illumination applications.

To calculate the gain, let us assume that a small voltage $\Delta V_{in} = V_{in-p} - V_{in-n}$ is applied to the opamp. The current flowing to the output will be $(g_{m1}\Delta V)/2 + (g_{m2}\Delta V)/2$, where g_m is small-signal voltage to current gain of transistors. The output resistance can be approximated as follows [22]:

$$R_{out} \approx \frac{1}{2} g_m {r_{ds}}^2 \tag{2}$$

where r_{ds} is small-signal drain-source resistance of the transistors. So, the total gain is:

$$\frac{V_{out}}{\Delta V} = R_{out} \times I_{out} = \left(\frac{1}{2} g_m {r_{ds}}^2\right)\left(\frac{g_{m1}}{2} + \frac{g_{m1}}{2}\right)$$

$$= \frac{1}{2} {g_m}^2 {r_{ds}}^2. \tag{3}$$

Bias current flows through R_1 and then M_{12} is mirrored in M_3, which provides the current of the input stage. It is also mirrored into $M_{4,5}$ throughout $M_{13,14}$. The bias voltage (V_{bias}) for the cascode stage is made out of a resistor ladder. Based on simulation, $V_{DD}/2$ value for V_{bias} provides almost a symmetric output swing.

As shown in Fig. 2, the second opamp does not have any local feedback. Thanks to the folded-cascode structure, the open loop transfer function of the second opamp can be approximated by a single-pole. Output resistance of this opamp together with input capacitance of the power transistor makes dominant pole of the system. The second pole is made by parasitic capacitance on node V_{in} and the resistor R_1. The R_1 was designed in such a way that places the second pole far enough from the first one. Thereby, the feedback loop becomes stable considering its loop gain.

2.3 Power Transistor

In the used BiCMOS7 process, a MOS transistor can provide a higher driving current for the LED compared to a BJT with the same area. Due to the process limitation, the minimum gate channel length is 2 μm. To improve area yield and decrease the parasitic resistance, an interdigitated NMOS structure was used. Each unit cell transistor has a total W/L $=$ 1800 μm /2 μm. Source and drain are five finger-shaped N^+ areas in P-substrate that makes layout of each unit a square (optimum balance between parasitic resistance and capacitance). A higher number of fingers reduces parasitic series resistance, but also increases parasitic capacitance. The final transistor was made out of four parallel units to supply the required output current (maximum 700 mA).

2.4 Blue-Selective Photodiode

For blue selective photodiode, a silicon stripe-shaped photodiode was previously introduced by the authors [7]. It improves the responsivity by increasing active depletion region and consequently reducing the effect of dead layer formation of the shallow junctions [23]. This photodiode with junction at 330 nm, achieved a very high selectivity to blue light. Its maximum responsivity at 480 nm wavelength fits to the blue light output of the target LED. The selectivity parameter (ratio of responsivity for different wavelengths) is 42 for wavelength of 470 nm compared to 1000 nm. The 3-D schematic and the measured responsivity vs. wavelength are given in Fig. 4(a) and (b), respectively.

In case of a different LED color, one may change the implantation parameter for the best junction depth. The easiest solution would be using the simple dual junction PNP structure which was also discussed in [7]. It can simply be used for longer wavelength and, if needed, to make the selectivity for target wavelength some color filtering coating (e.g., color photoresist coating) can be applied [24].

2.5 Target LED

The target LED in this study is a Bridgelux Blue Power Die, which is an InGaN-based blue color vertical LED. The LED dimension is 1143 $\times$ 1143 $\times$ 150 μm^3 and the maximum DC driving current is 700 mA. Dominant wavelength in nominal condition is in 450-470 nm range. It can be used for a broad range of applications including general illumination, street lights, portable lighting, architectural lighting, directional lighting, wide area lighting, display backlighting, digital camera flash, and automotive lighting, and the most remarkable one is lighting element in phosphor-based white LED package [25].

According to the LED datasheet [25], high junction temperature leads to forward voltage shift, light intensity decay, and wavelength shift, as shown in Fig. 5. The light intensity decays up to 20% and forward voltage changes up to –0.4 V at a junction temperature of 150 °C. Consequently, an integrated controlling block would have significant opportunities to enable a reliable light intensity and color temperature.

3. System Implementation

The complete package size is 4.5 $\times$ 10 mm^2. It integrates four LEDs on a silicon heat sink. The LEDs are connected in series and can be turned on with different combinations. This Si-based

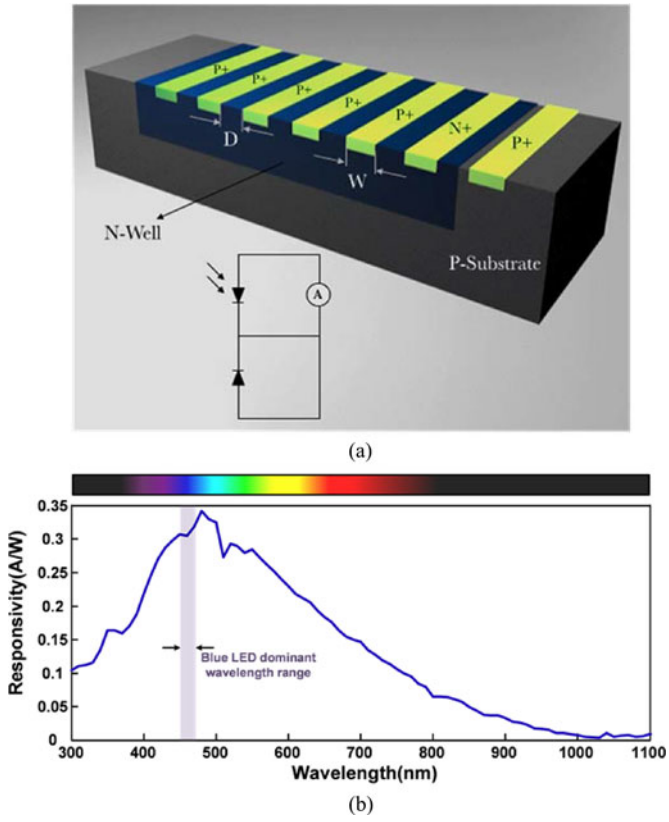

Fig. 4. (a) Three-dimensional schematic of blue selective photodiode and (b) responsivity vs. wavelength measurement result (the patterned inset shows the dominant wavelength of target LED).

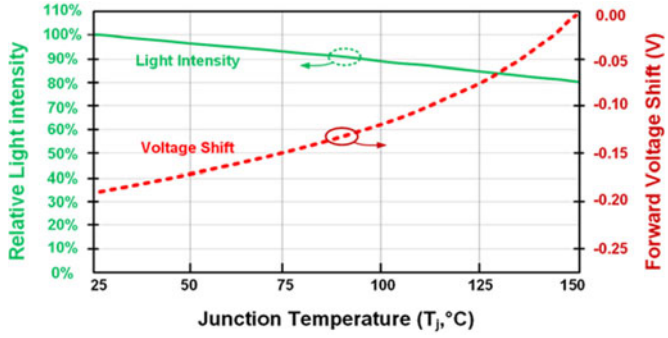

Fig. 5. Relative light intensity and forward voltage shift (normalized at 350 mA, $T_j = 25^\circ C$) versus junction temperature. The data was reproduced from datasheet [25].

high-power, high-lumen package can illuminate up to 1200 lumen at the output. There were also some more sensors and devices integrated (such as electrostatic discharge (ESD) protection diode, temperature sensor, and readout circuit) that are not in the scope of this paper. For each of the LEDs, there are sets of temperature and light sensors. Fig. 6(a) illustrates complete schematic of the package with components used on its test PCB. As it is shown, instead of using extra source for different inputs, just one V_{DD} was used and other inputs such as V_{CM}, I_{bias}, and V_{Ref} were made by external potentiometers. The layout and chip micrograph is given in Fig. 6(b).

The whole system was fabricated using the 2 μm 7-mask BiCMOS process with 2 metal layers. In this process, different devices such as silicon sensors, Bipolar and CMOS transistors for feedback control circuits can be implemented. Although the BiCMOS7 cannot fabricate advanced submicron

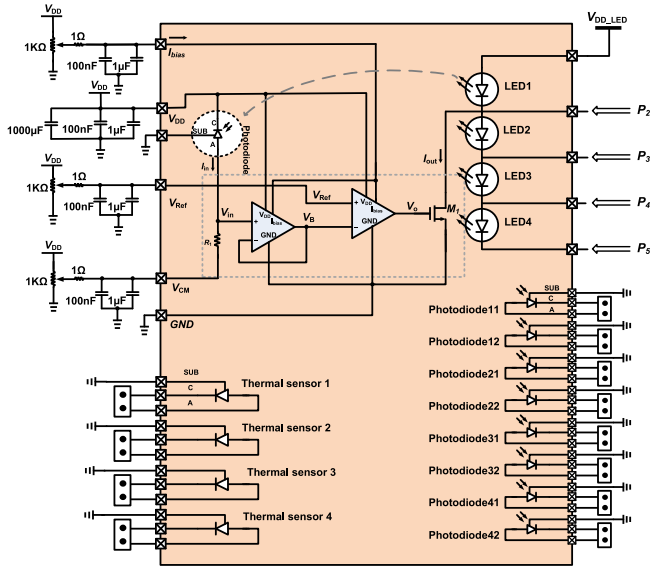

(a)

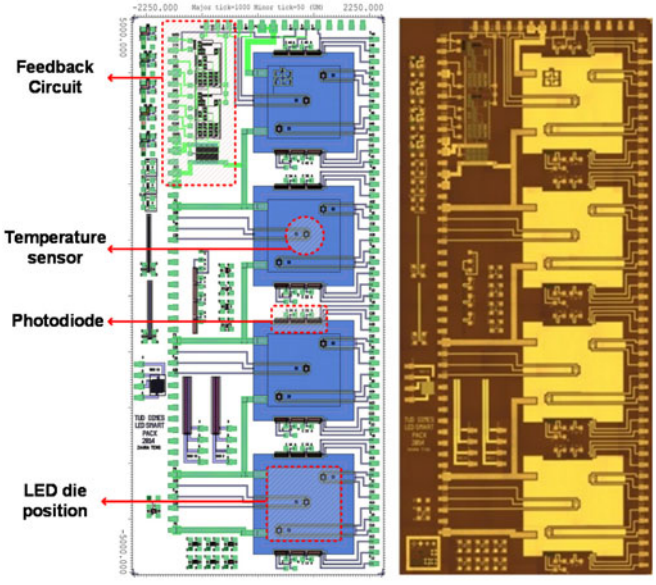

(b)

Fig. 6. (a) Schematic of the package and (b) layout and chip micrograph showing component positions in the package.

transistors due to size and process flow limitations, it is a relatively low-cost and straightforward process. It is also well appropriate for LED wafer level package (WLP) to integrate relative large area LED chips (in our case 1.1 $\times$ 1.1 mm^2). The seven masks include N-well, N$^+$ area, P$^+$ area, contact opening, first metal, via opening, and second metal. More details on BiCMOS process can be found in [7].

For process simplicity, metal gates instead of poly has been used in BiCMOS7. So, resistors were implemented with N$^+$ area in P-substrate. It should be mentioned that resistance of this type of resistor shows a small dependency on temperature, light, and bias conditions which should be considered in the design. Also, leakage current of a reverse biased PN junction (p-sub is grounded)

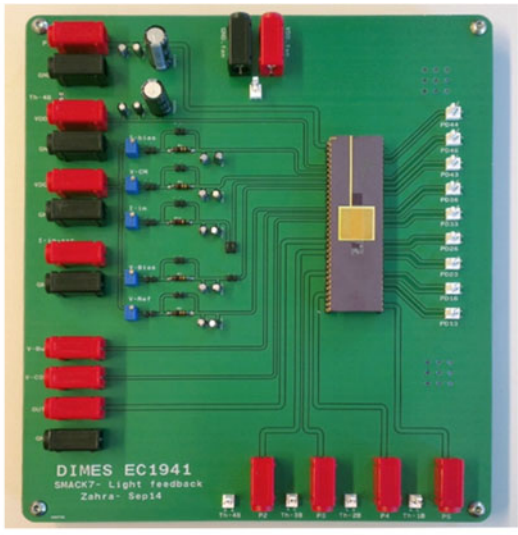

(a)

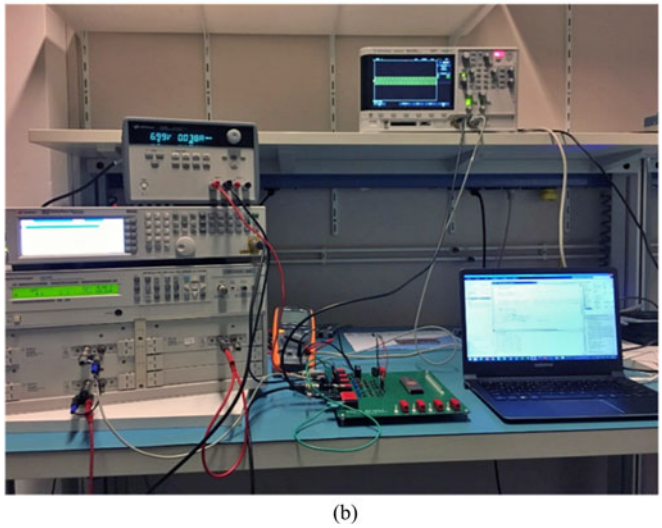

(b)

Fig. 7. (a) Designed PCB with assembled components and (b) measurement setup for the light feedback control circuit.

is always there but negligible in most of the designs. To have a simple and consistent layout design, all the transistors of the opamps are sized $W/L = 400\ \mu\text{m}/4\ \mu\text{m}$.

Transistor and device models were extracted from a sample run with same parameters and used for design and simulation. After preparing the Si package, it was diced, and LED dies were mounted (with a thermal-conductive glue) and wire bonded in predefined positions, on top of the temperature sensors, and next to the light sensors.

The PCB test board and characterization setup are shown in Fig. 7(a) and (b), respectively. In the real application, the PCB can be designed much smaller and uses SMD components and connectors.

4. Measurement Results

4.1 Opamps

Firstly, the opamps were characterized. For all the tests V_{DD} is set to 7 V and I_{bias} is 100 μA (total for the two opamps). Opamp #1 (see Fig. 2) is in unity gain feedback configuration (voltage buffer).

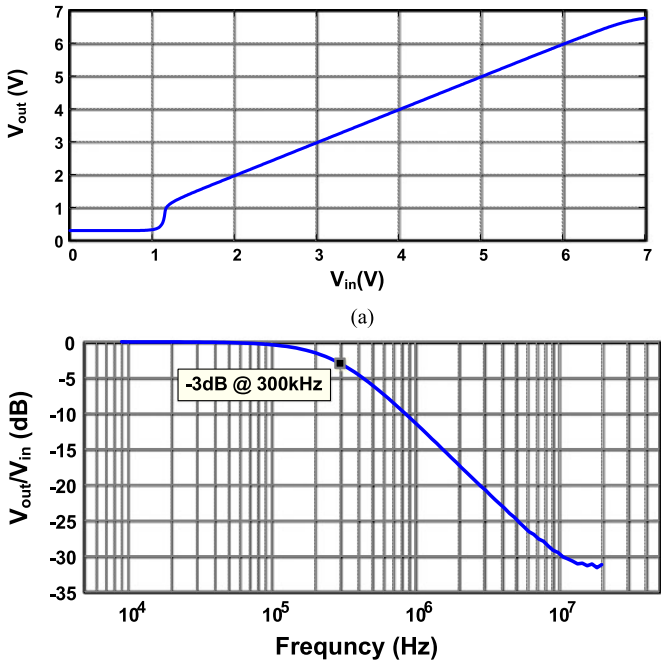

Fig. 8. (a) Input/output voltage characteristic and (b) frequency response of opamp #1.

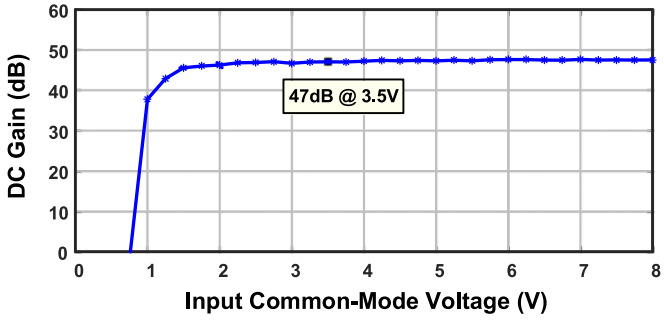

Fig. 9. DC gain of opamp #2 versus V_{CM}.

DC voltage on V_{in} node of the chip was swept from 0 V to V_{DD}, and the output of opamp #1 was measured. Based on results of this measurement which is shown in Fig. 8(a), the opamp achieved an input/output buffering range between 1.2 and 7 V. According to this result, V_{CM} can be set to 1.5 V to be always on the safe side for operating input range of the opamps. Fig. 8(b) shows measured frequency transfer function of opamp#1, including its output load (coming from input of opamp #2). In this test, a sinusoidal signal was applied to the input, and gain of the opamp was measured at different input frequencies. Based on the results, the opamp has 300 kHz unity gain bandwidth.

Opamp#2 is the main gain stage of the feedback system and is used in open loop configuration. To measure its open loop gain, its negative input (V_{in-n}: node V_B) was forced externally from a voltage source. Then, its positive input (V_{in-p}: node V_{Ref}) was swept in a range with very fine steps to measure the voltage gain to its output (V_O). Fig. 9 shows open-loop gain of the opamp versus common-mode input voltage. It has demonstrated 47 dB (224 x) gain for its typical operating points.

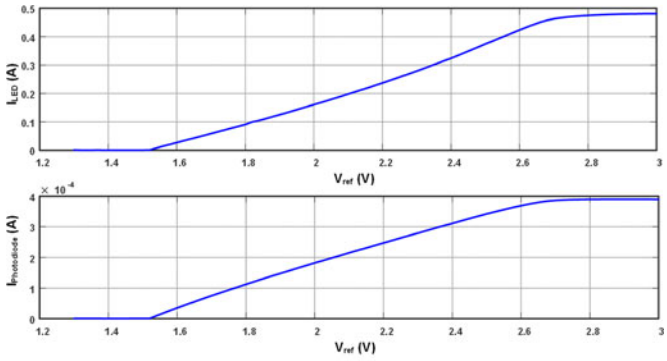

(a)

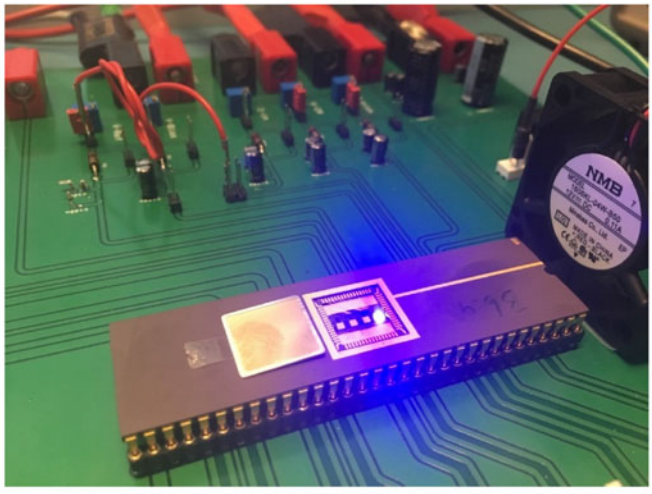

(b)

Fig. 10. (a) Feedback system characteristic, currents of LED and photodiode versus input reference voltage, and (b) a photo of the package while controlling the light output.

4.2 Feedback System

Second, the whole feedback loop was characterized. Feedback and controlling functionality of the system was investigated by a DC test. Input reference voltage (V_{Ref}) was swept from 1.3 V to 3 V, and output current of power transistor to the LED (I_{LED}) and current of photodiode were measured and are shown in Fig. 10(a). As V_{Ref} was increased from $V_{CM} = 1.5$ V, the feedback system operated such that light output of the LED and consequently the current of photodiode were increased linearly and proportionately. This is done through increasing output voltage of the feedback system (V_O) and output current of the power transistor (I_{LED}). In this way, light output of the LED is regulated. Each 0.1 V change in V_{Ref} as the input control voltage results in 33 μA change in $I_{photodiode}$ and 36 mA in LED driving current. As the reference voltage reaches to about 2.7 V, the current of photodiode stops tracking the input. The reason is that after that point, V_O has reached and saturated to V_{DD} and consequently output current of the power transistor is saturated. Note that nominal current of the LED is 350 mA. Fig. 10(b) shows the photo of the package while controlling the light output.

In the next step, dynamics of the feedback system was tested. While V_{CM} was set constantly to 1.5 V, V_{Ref} was instantly changed from 1.63 V to 1.83 V, corresponding to $\sim$50 mA and $\sim$100 mA of I_{LED}, respectively. As shown in Fig. 11, V_{out} tracked the change quite fast to set the light output to the new input (settling time of 1.87 μs). Based on this figure, cut-off frequency of the closed-loop feedback system is estimated to be about 680 kHz. Therefore, the control circuit is able to filter ripples on power supply source up to this frequency, far beyond the requirements of most of the

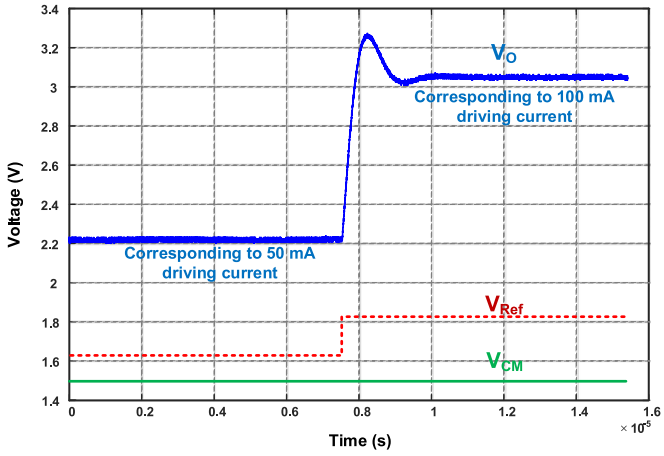

Fig. 11. Step response of feedback loop V_{Ref} is changed between 1.63–1.83 V.

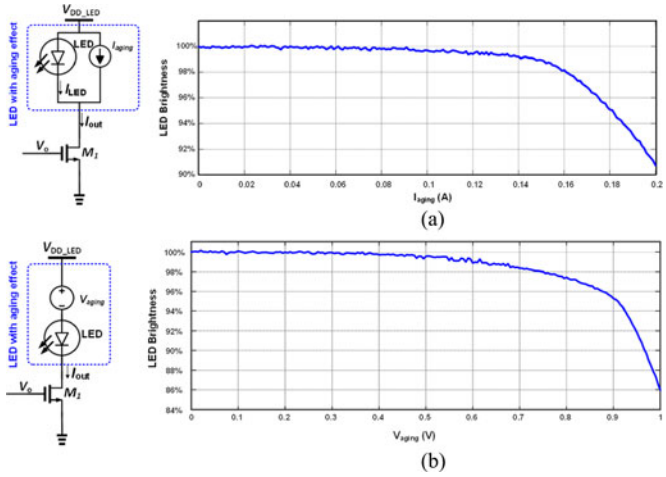

Fig. 12. Aging study (a) by modelling aging as a current source and (b) by modelling aging as a voltage source.

lighting applications. For instance, in general illumination application photometric ripples of more than 100 to 120 Hz are not visible to human eyes [18], [19], [26], [27].

4.3 Robustness Against Variations

Two different tests were performed to evaluate the accuracy and robustness of the feedback system against changes in the LED characteristics. In the first test, variations of the light intensity of the LED with current changes was considered. A common reason for this change could be LED aging, where the LED emits a lower light intensity for the same current over time [16], [17]. This can be modeled with an aging current source (I_{aging}) in parallel with a non-aged LED (see Fig. 12(a)). In this test, V_{Ref} was set in a way that the LED drains 100 mA net current. Then, the aging current was increased from 0 to 200 mA. Aging currents up to 150 mA decreased light intensity of the LED (calculated from measured current of the non-aged LED) by less than 1%.

In the second test, variation of the forward bias voltage to light intensity of the LED was investigated. The most common reasons for these changes could be change in junction temperature (as shown in Fig. 5), LED aging [5], and aging of the LED interconnects [28]. This was modeled with a voltage source (V_{aging}) in series with the original LED (see Fig. 12(b)). In this test, the aging voltage was swept from 0 to 1V, while V_{DD_LED} was set to 4.2 V. An aging voltage as high as 0.6 V

caused less than 1% reduction in the light intensity of LED. If V_{aging} increases even more, there is no voltage headroom left for drain-source of the power transistor and it goes to triode. Hence, the feedback system cannot compensate anymore. Note that a higher V_{DD_LED} can substantially improve robustness of the system against V_{aging} changes, while it degrades power efficiency of the whole package.

5. Conclusion

This work reports a successful monolithic integration of light output feedback control circuit in a blue/UV LED package. It is also a very appropriate solution for packaging a phosphor-based white LED module. Silicon-based wafer level smart control unit was integrated through our low-cost 7-mask BiCMOS process. For sensing blue/UV light in the package, optical sensors with peak responsivity at 480 nm wavelength were implemented. For controlling functions, a feedback circuit with a power transistor for driving the LED current were monolithically integrated. The opamp functionality was successfully tested with having 47 dB gain. The power transistor could provide up to 700 mA current. The whole feedback circuit could regulate light output based on a reference voltage with removing power supply ripples up to 680 kHz. Robustness of the feedback system was tested against changes in LED current/voltage to light intensity characteristics. Considering a tight error tolerance of 1%, the system was able to handle up to 150 mA and 0.6 V change in current and voltage characteristic of the LED while providing the same light intensity. Furthermore, it demonstrates the functionality of silicon-based smart LED packaging with stable light output, which can also be applied to other smart systems like interposer for high level electronics, MEMS, etc.

References

[1] Y.-C. Lin, J. P. You, N. T. Tran, Y. He, and F. G. Shi, "Packaging of phosphor based high power white LEDs: Effects of phosphor concentration and packaging configuration," *J. Electron. Packag.*, vol. 133, no. 1, 2011, Art. no. 11009.

[2] H. Luo, J. K. Kim, E. F. Schubert, J. Cho, C. Sone, and Y. Park, "Analysis of high-power packages for phosphor-based white-light-emitting diodes," *Appl. Phys. Lett.*, vol. 86, pp. 1–3, 2005.

[3] J. K. Kim, H. Luo, E. F. Schubert, J. Cho, C. Sone, and Y. Park, "Strongly enhanced phosphor efficiency in GaInN white light-emitting diodes using remote phosphor configuration and diffuse reflector cup," *Jpn. J. Appl. Phys. Part 2 Lett.*, vol. 44, nos. 20–23, pp. 649–651, 2005.

[4] S. Chhajed, Y. Xi, Y. L. Li, T. Gessmann, and E. F. Schubert, "Influence of junction temperature on chromaticity and color-rendering properties of trichromatic white-light sources based on light-emitting diodes," *J. Appl. Phys.*, vol. 97, no. 5, pp. 1–8, 2005.

[5] H. Chen *et al.*, "Failure analysis of electrical-thermal-optical characteristics of LEDs based on AlGaInP and InGaN/GaN," *Semiconductors*, vol. 46, no. 10, pp. 1333–1338, 2012.

[6] J. K. Kim and H. C. Lee, "A photo-sensor on thin polysilicon membrane embedded in wafer level package LED," *Proc. SPIE*, vol. 8431, pp. 8431–8437, 2012.

[7] Z. Kolahdouz, A. Rostamian, M. Kolahdouz, T. Ma, H. van Zeijl, and K. Zhang, "Output blue light evaluation for phosphor based smart white LED wafer level packages," *Opt. Exp.*, vol. 24, no. 4, pp. 174–177, 2016.

[8] W. K. Jeung *et al.*, "Silicon-based, multi-chip LED package," in *Proc. 57th Electron. Compon. Tech. Conf.*, 2007, pp. 722–727.

[9] C. T. Tsou and Y.-S. Huang, "Silicon-based packaging platform for light-emitting diode," *IEEE Trans. Adv. Packag.*, vol. 29, no. 3, pp. 607–614, Aug. 2006.

[10] L. Di Benedetto, M. Kolahdouz, B. G. Malm, M. Ostling, and H. H. Radamson, "Strain balance approach for optimized signal-to-noise ratio in SiGe quantum well bolometers," in *Proc. Eur. Solid State Device Res. Conf.*, 2009, pp. 101–104.

[11] J. Y. Andersson, P. Ericsson, H. H. Radamson, S. G. E. Wissmar, and M. Kolahdouz, "SiGe/Si quantum structures as a thermistor material for low cost IR microbolometer focal plane arrays," *Solid State Electron.*, vol. 60, no. 1, pp. 100–104, 2011.

[12] H. H. Radamson and L. Thylén, *Monolithic Nanoscale Photonics–Electronics Integration in Silicon and Other Group IV Elements*. Amsterdam, The Netherlands: Elsevier, 2014.

[13] S. Chang and C. Tsou, "A novel silicon-based LED packaging module with an integrated temperature sensor," *IEEE Trans. Compon., Packag. Manuf. Technol.*, vol. 4, no. 5, pp. 769–776, May 2014.

[14] S. Y. R. Hui, S. N. Li, X. H. Tao, W. Chen, and W. M. Ng, "A novel passive offline LED driver with long lifetime," *IEEE Trans. Power Electron.*, vol. 25, no. 10, pp. 2665–2672, Oct. 2010.

[15] K. Tseng and C. Tsou, "Novel silicon-based led packaging module with an integrated photosensing element," *IEEE Photon. Technol. Lett.*, vol. 25, no. 5, pp. 515–518, Mar. 2013.

[16] ETAP Lighting, "LED lifetime in practice–The ETAP approach," 2009. [Online]. Available: http://www.etaplighting.com/uploadedFiles/Downloadable_documentation/documentatie/whitepaper_LED_EN.pdf

[17] "Calculate reliable LED lifetime performance in optocouplers," 2014. [Online]. Available: http://www.avagotech.com/docs/AV02-3401EN
[18] P. Di Maso. (Texas Instruments), "The impact of low frequency ripple current on LEDs and LED drivers," 2010. [Online]. Available: https://www.ledlightforyou.com/Downloads/data/Publications/TI-The-Impact-of-Low-Frequency-Ripple-Current-on-LEDs-and-LED-Drivers-10–28-2010.pdf. [Accessed: Sep. 7, 2016].
[19] F. Zhang, J. Ni, and Y. Yu, "High power factor AC-DC LED driver with film capacitors," *IEEE Trans. Power Electron.*, vol. 28, no. 10, pp. 4831–4840, Oct. 2013.
[20] M. A. Dalla Costa, M. F. de Melo, J. M. Alonso, W. D. Vizzotto, and L. Chies, "Analysis of low-frequency current ripple transmission in series-resonant LED drivers," *Electron. Lett.*, vol. 51, no. 9, pp. 716–717, 2015.
[21] B. Razavi, *Design of Analog CMOS Integrated Circuits*. New York, NY, USA: Tata McGraw-Hill, 2002.
[22] T. C. Carusone, D. Johns, and K. Martin, *Analog Integrated Circuit Design*. New York, NY, USA: Wiley, 2011.
[23] M. Kermaniha *et al.*, "Systematic optimization of phosphorous diffusion for solar cell application," *J. Mater. Sci. Mater. Electron.*, vol. 27, no. 12, pp. 13086–13092, 2016.
[24] C. Chen and C. Tsou, "Silicon-based white LED packaging module with an integrated RGB color sensor," *IEEE Photon. Technol. Lett.*, vol. 27, no. 5, pp. 553–556, Mar. 2015.
[25] Bridgelux, Bridgelux BXCD45 Product Data Sheet DS-C15 (10/22/2012), Revision C., Bridgelux Inc., Livermore, CA, USA, 2012.
[26] M. J. Mayer, C. B. Kim, A. Svingos, and A. Glucs, "Foveal flicker sensitivity in healthy aging eyes. I. Compensating for pupil variation," *J. Opt. Soc. Amer. A.*, vol. 5, no. 12, pp. 2201–2209, 1988.
[27] H. De Lange Dzn, "Research into the dynamic nature of the human fovea–Cortex systems with intermittent and modulated light. II. Phase shift in brightness and delay in color perception," *J. Opt. Soc. Amer.*, vol. 48, no. 11, pp. 784–789, 1958.
[28] L. Zhang *et al.*, "Study on ag-plated cu lead frame and its effect to LED performance under thermal aging," *IEEE Trans. Device Mater. Rel.*, vol. 14, no. 4, pp. 1022–1030, Dec. 2014.